

Ultra high energy cosmic rays from past activity of Andromeda galaxy

V. N. Zirakashvili,^{*} V. S. Ptuskin, and S.I.Rogovaya

Pushkov Institute of Terrestrial Magnetism, Ionosphere and Radiowave Propagation, 108840, Troitsk, Moscow, Russia

Accepted 2022 November 8. Received 2022 October 25; in original form 2022 September 21

ABSTRACT

It is shown that the relativistic jets associated with the growth and past activity of the supermassive black hole in the Andromeda galaxy could be the main source of cosmic rays with energies above 10^{15} eV. Most of the cosmic ray energy is related to a bow shock of the jet that produces multi-PeV cosmic rays with light composition. The highest energy cosmic rays with heavy composition are produced in the jet itself. The spectra of energetic particles produced in Andromeda galaxy and propagated to the Earth are calculated and compared with observations.

Key words: cosmic rays – acceleration of particles – jets – supermassive black holes

1 INTRODUCTION

It is believed that the acceleration of ultra-high energy cosmic rays (UHECRs) occurs in astrophysical objects with relativistic motions. This is happening in pulsar nebula, active galactic nuclei (AGN) jets driven by the gas accretion onto central black holes, and anisotropic explosions of gamma-ray bursts (see a review of Bykov et al. (2012)).

It is currently clear, that the energy released during the gas accretion and the corresponding growth of supermassive black holes (SMBHs) produce a strong impact on the evolution of parent galaxies (e.g. Donahue & Voit (2022)). If the power of the jet driven by accretion is high enough the jet can propagate on sub-Mpc scales in the circumgalactic medium. The particles can be accelerated in the magnetosphere of rotating SMBH (Istomin & Sol 2009; Bañados et al. 2009; Jacobson & Sotiriou 2010; Wei et al. 2010), near the jet boundary via shear acceleration, at the inner termination shock at the end of the jet, and the outer bow shock surrounding the cocoon of the jet (Norman et al. 1995).

Taking into account different acceleration sites and different acceleration mechanisms one can expect several different components in the general flux of emitted accelerated particles.

In particular, the spectra of energetic particles produced at the outer bow shock of the jet via the diffusive shock acceleration (DSA) mechanism are similar to the spectra of galactic supernova remnants (SNRs). It is known that the DSA mechanism (Krymskii 1977; Bell 1978; Axford et al. 1977; Blandford & Ostriker 1978) operates in the vicinity of shocks in SNRs. The X-ray and gamma-ray observations of the last decades indicated the presence of multi-TeV energetic particles in these objects (see e.g. Lemoine-Goumard (2014) for a review).

The light chemical composition of cosmic rays accelerated at the bow shock is expected because of the low metallicity and high ionization state of the circumgalactic medium.

The heavier composition and different spectra are expected for particles accelerated in the jet itself. Acceleration of particles in the

shear flow (Berezhko 1981; Earl et al. 1988) is one of the possibilities. The presence of electrons accelerated up to PeV energies in shear flows is consistent with modern X-ray and gamma-ray observations of large-scale extragalactic jets (Wang et al. 2021). It is expected that protons and nuclei can be accelerated to higher energies because of the lower energy losses.

Probably the jets with strong toroidal magnetic fields produce the highest energy particles while the maximum energy of particles accelerated by bow shocks is lower. Low-energy particles can propagate only from nearby sources. The prime candidates are SMBHs in the Galactic center and the Andromeda galaxy with masses $4 \cdot 10^6 M_{\odot}$ and $2 \cdot 10^8 M_{\odot}$ respectively. They are not in an active state now. However, they were active in past. The huge gamma ray halo of Andromeda galaxy (Karwin et al. 2019), Fermi and eROSITA bubbles (Su et al. 2010; Predehl et al. 2020) in the Milky Way are apparently originated as a result of recent activity of the central SMBHs. Cosmological simulations of Andromeda-like galaxies (Pillepich et al. 2021) also demonstrate a pulsed activity of SMBH every 10^8 years and the peak mechanical luminosity about 10^{44} erg s^{-1} .

The idea of the cosmic ray production during the past activity of the Galactic center is not new (see e.g. Ptuskin & Khazan (1981); Giler (1983); Istomin (2014); Fujita et al. (2017)). The particles above the "knee" energies could be also produced in other objects like Galactic winds (e.g. Völk & Zirakashvili (2004)), peculiar supernovae (e.g. Wang et al. (2007)), and neutron star mergers (Kimura et al. 2018b).

In the present paper we calculate the propagation of UHECRs from Galactic center and nearby Andromeda galaxy and check whether they can considerably contribute to the observed spectrum of UHECRs.

The paper is organized as follows. In the next Sections 2 and 3, we describe our model. The application of the model for Andromeda and Milky Way is given in Section 4. The discussion of results and conclusions are presented in Sections 5 and 6.

^{*} E-mail: zirak@izmiran.ru

2 PROPAGATION MODEL

The evolution of energy distributions of protons $N(\mathbf{r}, z, \varepsilon)$ and nuclei $N_i(\mathbf{r}, z, \varepsilon, A)$ in expanding Universe is described by equations (Berezinsky & Gazizov 2006)

$$-H(z)(z+1)\frac{\partial N}{\partial z} = \nabla D(\mathbf{r}, z, \varepsilon)(z+1)^2 \nabla N + H(z) \left(\varepsilon \frac{\partial N}{\partial \varepsilon} - 2N \right) + \frac{\partial}{\partial \varepsilon} b(\varepsilon)N + 4v_{ph}(4)N_i(4) + \sum_{A=5}^{56} v_{ph}(A)N_i(A) + q(z, \varepsilon)(1+z)^3 \delta(\mathbf{r}), \quad (1)$$

$$\begin{aligned} -H(z)(z+1)\frac{\partial N_i(A)}{\partial z} &= \nabla D_i(\mathbf{r}, z, \varepsilon)(z+1)^2 \nabla N_i(A) \\ &+ H(z) \left(\varepsilon \frac{\partial N_i(A)}{\partial \varepsilon} - 2N_i(A) \right) + \frac{\partial}{\partial \varepsilon} b(\varepsilon)N_i(A) \\ &- v_{ph}(A)N_i(A) + v_{ph}(A+1)N_i(A+1) + q_i(z, \varepsilon, A)(1+z)^3 \delta(\mathbf{r}). \quad (2) \end{aligned}$$

Here \mathbf{r} is the comoving coordinate, and the redshift z is used instead of time. This system for all kinds of nuclei with different mass numbers A from Iron to Hydrogen should be solved simultaneously. The energy per nucleon $\varepsilon = E/A$ is used here because it is approximately conserved in a process of nuclear photodisintegration, $q(z, \varepsilon)$ and $q_i(z, \varepsilon, A)$ are the spectra of the point cosmic-ray proton and nuclei sources respectively, $b(A, \varepsilon, z)$ is the characteristic rate of energy loss by the production of e^-e^+ pairs and pions, $v_{ph}(A, \varepsilon, z)$ is the frequency of nuclear photodisintegration (for details see our paper Ptuskin et al. (2013)), the sum in the right side of Eq. (1) describes the contribution of secondary protons produced by the photodisintegration of heavier nuclei, $H(z) = H_0((1+z)^3 \Omega_m + \Omega_\Lambda)^{1/2}$ is the Hubble parameter in a flat universe with the matter density $\Omega_m (= 0.3)$ and the Λ -term $\Omega_\Lambda (= 0.7)$, its value $H_0 = 70 \text{ km s}^{-1} \text{ Mpc}^{-1}$ at current epoch is used.

Diffusion coefficient $D(\mathbf{r}, z, E)$ is determined by scattering on magnetic inhomogeneities. We use the analytical approximation obtained in numerical trajectory calculations of Harari et al. (2014).

$$D = \frac{cl_c}{3} \left(4 \frac{E^2}{E_c^2} + 0.9 \frac{E}{E_c} + 0.23 \frac{E^{1/3}}{E_c^{1/3}} \right), \quad E_c = ZeBlc \quad (3)$$

where $B \propto (1+z)^2$ is the magnetic field strength and $l_c \propto (1+z)^{-1}$ is the coherence scale of the magnetic field in the intergalactic medium.

3 PARTICLE ACCELERATION IN JETS

A relativistic jet outflow produces complex flow structures in the galactic halo schematically shown in Fig.1 (see, for example, modeling of Seo et al. (2021)). The supersonic jet flow terminates at the end of the jet and produces a low density cocoon with the backward flow. The cocoon is surrounded by the denser galactic halo gas shocked at the bow shock. The bow shock propagates at a non-relativistic speed depending on the ratio of the jet and halo gas densities. DSA mechanism can operate at the bow shock, at the termination shock at the end of the jet, and in multiple small scale shocks inside the bow shock and cocoon observed in numerical modeling of jets (Seo et al. 2021). The presence of the shear flow in the cocoon and in the jet itself probably results in the shear acceleration. Below we shall consider 3 main components of accelerated particles.

1) The particles accelerated up to maximum energies in the jet

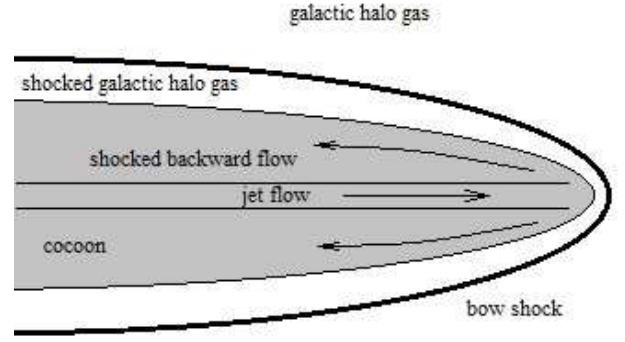


Figure 1. Schematical view of the jet.

Table 1. Parameters of source components in Andromeda galaxy

component	γ	ε_{\max}	$L_{\text{cr}}(z=0)$	$k(A)$
jet	0.5	10^{19} eV	$1.3 \cdot 10^{40} \text{ erg s}^{-1}$	$90k_{\odot}(A), A > 4$
bow shock	2.0	$5 \cdot 10^{15} \text{ eV}$	$3.2 \cdot 10^{42} \text{ erg s}^{-1}$	$k_{\odot}(A)A/Z$
cocoon	2.0	$6 \cdot 10^{17} \text{ eV}$	$1.4 \cdot 10^{41} \text{ erg s}^{-1}$	$k_{\odot}(A)A/Z$

itself via shear acceleration, DSA at the termination shock, or instabilities in the jet.

2) The particles with the lowest maximum energies are accelerated at the non-relativistic bow shock. The properties of this component are robust because DSA is well studied.

3) The particles accelerated up to intermediary energies in the cocoon where the shear acceleration in sub-relativistic backward flow occurs.

The source spectra of different components are given by

$$q(\varepsilon, A) \propto k(A)\varepsilon^{-\gamma} \exp\left(-\frac{A\varepsilon}{Z\varepsilon_{\max}}\right) \quad (4)$$

where the function $k(A)$ describes the source chemical composition and can be written in terms of the solar composition $k_{\odot}(A)$.

The spectral index γ , the maximum energy ε_{\max} and coefficients $k(A)$ adjusted to reproduce observational data are given in Table 1, see also Section 5 below.

The injection of particles into DSA depends mainly on the ratio of atomic mass to the charge. Hybrid modeling of quasi-parallel shocks shows that the injection is proportional to this quantity (Caprioli et al. 2017). Galactic cosmic ray composition then can be reproduced if ions are injected in the neutral or warm interstellar medium where they are single- or double-ionized. In the case of the hot medium of the galactic halo or the hot cocoon interior, the full ionization of ions is a more reasonable assumption. So we use a weak enhancement factor of injection A/Z for the bow shock and cocoon components. This results in light cosmic ray composition. The use of a similar enhancement for the cocoon component is justified if the injection occurs in small-scale shocks in the cocoon or if the bow shock particles are reaccelerated in the cocoon. The latter opportunity seems very likely because the halo gas shocked at the bow shock is mixed with the cocoon material due to development of the Kelvin-Helmholtz instability in the shear flow (see Mbarek & Caprioli (2019)).

A similar injection mechanism can operate for the jet component when a small number of cocoon particles can be further reac-

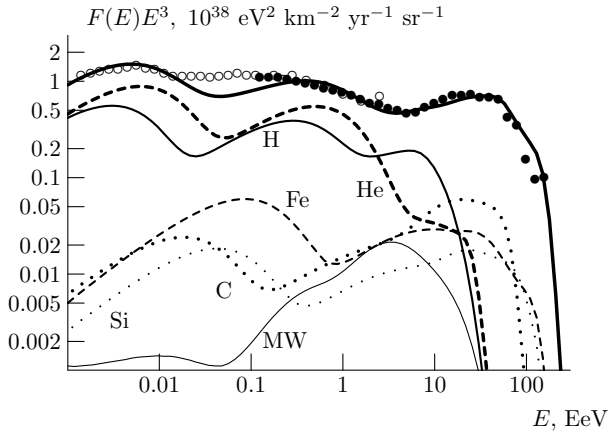


Figure 2. Spectra of different elements and all-particle spectrum (thick solid line) produced in Andromeda galaxy and observed at the Earth position. A possible contribution in the all particle spectrum from the Galactic center (MW) is shown by the thin solid line. Spectra of Tunka-25, Tunka-133 array (Budnev et al. (2020), open circles) and Pierre Auger Collaboration (Abreu et al. (2021), energy shift +10%, black circles) are also shown.

celerated in the jet. Since the shear acceleration is very effective and produces the hardest spectra in ultra-relativistic flows (see e.g. Rieger & Duffy (2019); Wang et al. (2021)) we expect that jet particles are mainly produced from reacceleration of the bow shock component in the ultra-relativistic part of the jet. Usually the jet is ultra-relativistic at sub-kiloparsec scales and becomes slower at larger distances (see Blandford et al. (2019) for a review). Therefore the jet component is produced closer to the jet origin and its composition is heavy because of the high metallicity of galactic bulges and preferential injection of partially ionized heavy ions into DSA at the bow shock. Qualitatively speaking, the large adjusted enrichment factor 90 of the jet component (see Table 1) is the product of the high metallicity of the galactic bulge 3-5 and the enhancement factor 10-20 of the ion injection at the bow shock.

4 MODELING MILKY WAY AND ANDROMEDA GALAXY

4.1 Andromeda galaxy

We model the propagation of particles from Andromeda galaxy at distance of 785 kpc from the maximum redshift $z = 1$ down to the present time $z = 0$. It was assumed that the enhanced SMBH accretion produced jet every 280 million years ($\Delta z = 0.02$) with the last episode 140 million years ago ($z = 0.01$). In addition we multiply the source terms in Eqs. (1,2) by $(1+z)^4$ to take into account cosmological evolution. Averaged in time luminosity L_{cr} of different components of accelerated particles are given in Table 1. We use the value of the intergalactic magnetic field $B = 10^{-7}$ G and the coherence scale $l_c = 0.13$ Mpc that gives $E_c = 1.2 \cdot 10^{19} Z$ eV. The particle distribution vanishes at the spherical boundary of simulation domain with radius $R = 8$ Mpc that corresponds to the escape of particles from the edge of the Local Supercluster of galaxies.

The numerical solution of cosmic-ray transport Eqs (1,2) follows the finite difference method. The results of calculations are shown in Figures (2-4).

The calculated all-particle spectrum and spectra of protons and nuclei are shown in Figure 2. The photodisintegration of nuclei on the background microwave photons strongly influences the high en-

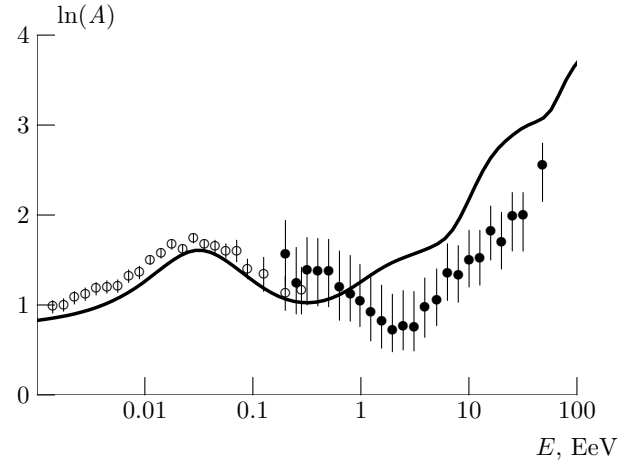


Figure 3. Calculated mean logarithm of atomic number A (solid line). The measurements of Tunka-133, TAIGA-HiSCORE array (Prosin et al. (2022) open circles) and Pierre Auger Collaboration (EPOS-LHC, energy shift +10% Bellido et al. (2017), black circles) are also shown.

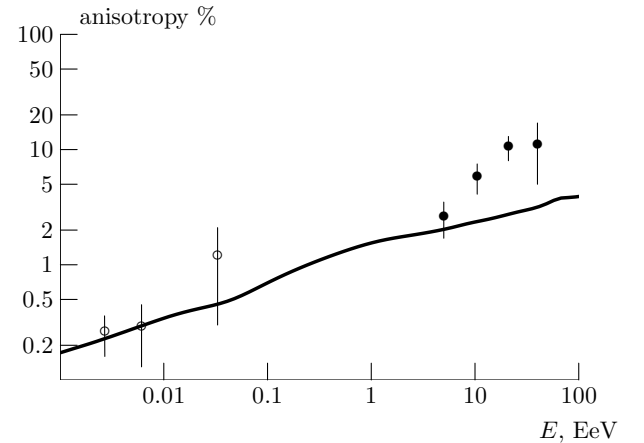


Figure 4. Calculated cosmic ray anisotropy (solid line). The results of Pierre Auger Collaboration (energy shift +10%, Aab et al. (2018) black circles) and KASCADE-Grande experiment (Chiavassa et al. (2015) open circles) are also shown.

ergy part of the all-particle spectrum. Taking into account the simplicity of the model the agreement with observations is good. A slightly heavier composition of the bow shock component would improve the fit at energies $10^{16} - 10^{17}$ eV. The same is true for the calculated mean logarithm A as shown in Figure 3. The slightly heavier composition is indeed expected because a small fraction of the time the bow shock propagates in the galactic bulge where gas is not fully ionized and the gas metallicity is high. Some input of reacceleration of heavy galactic cosmic ray component (Caprioli 2015; Kimura et al. 2018a) is not excluded either.

The calculated anisotropy is shown in Figure 4. It is low even despite the large free path of particles that is comparable to Andromeda distance for energies above $10^{19} Z$ eV. However the particles traveled to multi-Mpc distances during the time from the last SMBH activity and this explains the almost isotropic distribution at present.

4.2 Milky Way

We also model the propagation from SMBH in the Galactic center that was treated as the scaled Andromeda case. Assuming that the jet power is proportional to the accretion rate that in turn is proportional to the square of the SMBH mass (Bondi 1952) we divide the power L_{cr} of the jet, bow shock, and cocoon components by 50². The corresponding maximum energies were divided by 50. In addition, we use the last episode of the Galactic SMBH activity 28 million years ago ($z = 0.002$) which roughly corresponds to the age of the eROSITA bubbles (Predehl et al. 2020). The corresponding all-particle spectrum is shown in Figure 2.

5 DISCUSSION

The maximum energy of particles accelerated at the nonrelativistic bow shock is determined by the nonresonant cosmic ray streaming instability (Bell 2004) (see Appendix for details)

$$\begin{aligned} \epsilon_{\text{max}}^b &= \frac{\eta_{\text{esc}}}{2 \ln(B/B_b)} e \sqrt{\beta_{\text{head}} L_j c^{-1}} \\ &= 1.73 \cdot 10^{19} \text{ eV} \frac{\eta_{\text{esc}}}{2 \ln(B/B_b)} \beta_{\text{head}}^{1/2} \left(\frac{L_j}{10^{44} \text{ erg s}^{-1}} \right)^{1/2} \end{aligned} \quad (5)$$

Here β_{head} is the ratio of the speed of bow shock "head" to the speed of light c , L_j is the total power of two opposite directed jets, η_{esc} is the ratio of the energy flux of runaway accelerated particles to the kinetic flux of the shock. The logarithmic factor in the denominator corresponds to the situation when the seed magnetic field B_b amplified in the upstream region of the shock up to values of B via cosmic ray streaming instability.

The parameter η_{esc} is close to 0.01 for shocks where the pressure of accelerated particles is of the order of 0.1 of the shock ram pressure and can be higher at cosmic-ray modified shocks. For $\eta_{\text{esc}} = 0.01$, $\beta_{\text{head}} = 0.1$ and $\ln(B/B_b) = 5$ the protons are accelerated up to multi PeV energies at the jet bow shocks.

Our modeling shows that particles with energies above 10^{15} eV can be extragalactic. Lower energy particles are probably produced in Galactic supernova remnants.

We found the mean jet cosmic ray power of the order $3 \cdot 10^{42}$ erg s⁻¹ at the present epoch in the Andromeda galaxy. Taking into account the standard 10 % efficiency of DSA we expect the total mean jet power $3 \cdot 10^{43}$ erg s⁻¹. Then for 10% duty cycle the real jet power produced in an active state will be of the order of $3 \cdot 10^{44}$ erg s⁻¹ which is one percent of the Eddington luminosity. The peak luminosity could be correspondingly higher for shorter duty cycle of the order of 1% (Bird et al. 2008). Multi-PeV particles indeed can be produced at jet bow shocks in Andromeda galaxy. It takes cosmological time for these particles to reach the Earth. In this regard pulsations of the source do not play a role at these low energies. This is opposite to the highest energy part of the spectrum which is mainly determined by the last episode of SMBH activity.

The remnants of the cocoon and bow shock produced during the last episode are still in Andromeda's halo at hundred kpc distances (see, for example, the recent modeling of Huško & Lacey (2022)). The electrons are accelerated up to TeV energies at the bow shock with the speed of the order of 10^3 km s⁻¹ and produce gamma rays via Compton scattering of microwave background photons. The bow shock gamma-ray luminosity is of the order of the electron bow shock production power. Using a proton to electron ratio 10^3 that

is a characteristic value in young SNRs and the bow shock cosmic ray energetics $3 \cdot 10^{42}$ erg s⁻¹ mentioned above we obtain the bow shock gamma-ray luminosity $3 \cdot 10^{39}$ erg s⁻¹ that is in accordance with observations of Andromeda's gamma-ray halo (Recchia et al. 2021). Strong electron energy losses will result in the shell morphology of the gamma-emission (see also Recchia et al. (2021) for details).

The scaled jet power in the Galactic center is of the order of 10^{41} erg s⁻¹ in the active state that is exactly what is needed for the production of eROSITA bubbles (Predehl et al. 2020). With such energetics the Galactic center gives a small contribution in observed all particle spectrum (see Figure 2). We leave a detail treatment of the Galactic center's contribution for future investigations.

It is known that the electric potential difference is a reasonable estimate for the maximum energy of particles accelerated at quasi-perpendicular shocks (Zirakashvili & Ptuskin 2018). For example, single charged anomalous cosmic rays are accelerated up to hundreds MeV at the solar wind termination shock with the electric potential 200 MV (Cummings & Stone 1987). The jet electric potential is also a good estimate for the maximum energy as seen in trajectory calculations (Alves et al. 2018; Mbarek & Caprioli 2019).

It is given by

$$\begin{aligned} \epsilon_{\text{max}}^j &= e \sqrt{\beta_j L_{\text{mag}} c^{-1}} \\ &= 1.73 \cdot 10^{19} \text{ eV} \beta_j^{1/2} \left(\frac{L_{\text{mag}}}{10^{44} \text{ erg s}^{-1}} \right)^{1/2} \end{aligned} \quad (6)$$

where L_{mag} is the magnetic luminosity of two opposite jets.

So the maximum energy of the jet component 10^{19} eV used in our calculation is also in agreement with theoretical expectations.

Our model does not exclude a contribution at the highest energies from more distant sources like Cen A or M87. For example, Mollerach & Roulet (2019) use similar propagation parameters and showed that UHECRs can originate in Cen A.

It is known that the dipole anisotropy of the Auger Collaboration is in the direction of Cen A (Aab et al. 2018). Note that the direction of the anisotropy does not necessarily coincide to the direction of the main source. It could be that the particles produced during the last event in Andromeda are distributed isotropically within several Mpc now while the currently active Cen A source produces the observed anisotropy. In addition, there are several other "hot spots". In particular, the Telescope Array Collaboration reported the detection of the "hot spot" in the direction of the Perseus-Pisces supercluster (Kim et al. 2022). The Andromeda galaxy is in the same direction. So we can not exclude that this excess is related to Andromeda (see also the recent paper of Plotko et al. (2022)).

6 CONCLUSION

Our results and conclusions are the following:

1) We performed the modeling of the propagation of UHECRs produced in the Galactic center and in the nearby Andromeda galaxy. It was assumed that the periodic activity of the central SMBHs produces large-scale jets accelerating high energy particles.

2) We found that the light intermediary energy component of the jet cocoon produced via shear acceleration mechanism can explain the observable spectrum and composition below the "ankle". Heavier higher energy component with hard spectrum is probably produced in the jet itself.

3) Lowest energy light component related to particles accelerated

at the bow shock can explain the cosmic ray spectrum at PeV energies.

4) The Andromeda's gamma-ray halo is produced by electrons currently accelerated at the bow shock propagating in the galactic halo.

5) The production of UHECRs in Andromeda galaxy can explain the "hot spot" observed by Telescope Array Collaboration (Kim et al. 2022).

6) We suggest some modification of the reacceleration of galactic cosmic rays by jets (Caprioli 2015; Kimura et al. 2018a). It seems that the reacceleration of bow shock particles makes the main contribution to the production of UHECRs. The heavy composition is expected because the reacceleration efficiency is highest for ultra-relativistic jets. This happens close to the jet origin in the galactic bulge where the gas is partially ionized and has a high metallicity.

ACKNOWLEDGEMENTS

We thank the anonymous referee for useful comments. The work was partly performed at the Unique scientific installation "Astrophysical Complex of MSU-ISU" (agreement 13.UNU.21.0007).

DATA AVAILABILITY

All results in this paper were obtained using available published data.

REFERENCES

- Aab A., et al., 2018, *ApJ*, 868, 4
 Abreu P., et al., 2021, *Eur. Phys. J. C*, 81, 966
 Alves E. P., Zrake J., Fiuza F., 2018, *Phys. Rev. Lett.*, 121, 245101
 Axford W. I., Leer E., Skadron G., 1977, in *International Cosmic Ray Conference*. p. 132
 Bañados M., Silk J., West S. M., 2009, *Phys. Rev. Lett.*, 103, 111102
 Bell A. R., 1978, *MNRAS*, 182, 147
 Bell A. R., 2004, *MNRAS*, 353, 550
 Bell A. R., Schure K. M., Reville B., Giacinti G., 2013, *MNRAS*, 431, 415
 Bellido J., et al., 2017, arXiv e-prints, p. arXiv:1708.06592
 Berezhko E. G., 1981, *ZhETF Pisma Redaktsiiu*, 33, 416
 Berezhinsky V., Gazizov A. Z., 2006, *ApJ*, 643, 8
 Bird J., Martini P., Kaiser C., 2008, *ApJ*, 676, 147
 Blandford R. D., Ostriker J. P., 1978, *ApJ*, 221, L29
 Blandford R., Meier D., Readhead A., 2019, *ARA&A*, 57, 467
 Bondi H., 1952, *MNRAS*, 112, 195
 Budnev N. M., et al., 2020, *Astropart. Phys.*, 117, 102406
 Bykov A., Gehrels N., Krawczynski H., Lemoine M., Pelletier G., Pohl M., 2012, *Space Sci. Rev.*, 173, 309
 Caprioli D., 2015, *ApJ*, 811, L38
 Caprioli D., Yi D. T., Spitkovsky A., 2017, *Phys. Rev. Lett.*, 119, 171101
 Chiavassa A., et al., 2015, in *34th International Cosmic Ray Conference (ICRC2015)*. p. 281, doi:10.22323/1.236.0281
 Cummings A. C., Stone E. C., 1987, in *International Cosmic Ray Conference*. p. 421
 Donahue M., Voit G. M., 2022, *Physics Reports*, 973, 1
 Earl J. A., Jokipii J. R., Morfill G., 1988, *ApJ*, 331, L91
 Fujita Y., Murase K., Kimura S. S., 2017, *J. Cosmology Astropart. Phys.*, 2017, 037
 Giler M., 1983, *Journal of Physics G: Nuclear Physics*, 9, 1139
 Harari D., Mollerach S., Roulet E., 2014, *Phys. Rev. D*, 89, 123001
 Huško F., Lacey C. G., 2022, arXiv e-prints, p. arXiv:2208.09393
 Istomin Y., 2014, *New Astronomy*, 27, 13
 Istomin Y. N., Sol H., 2009, *Ap&SS*, 321, 57

- Jacobson T., Sotiriou T. P., 2010, *Phys. Rev. Lett.*, 104, 021101
 Karwin C. M., Murgia S., Campbell S., Moskalenko I. V., 2019, *ApJ*, 880, 95
 Kim J., Ivanov D., Kawata K., Sagawa H., Thomson G., 2022, in *37th International Cosmic Ray Conference*. p. 328, doi:10.22323/1.395.0328
 Kimura S. S., Murase K., Zhang B. T., 2018a, *Phys. Rev. D*, 97, 023026
 Kimura S. S., Murase K., Mészáros P., 2018b, *ApJ*, 866, 51
 Krymskii G. F., 1977, *Soviet Physics Doklady*, 22, 327
 Lemoine-Goumard M., 2014, in Ray A., McCray R. A., eds, *Proceedings of the International Astronomical Union Vol. 296, Supernova Environmental Impacts*. pp 287–294, doi:10.1017/S1743921313009605
 Mbarek R., Caprioli D., 2019, *ApJ*, 886, 8
 Mollerach S., Roulet E., 2019, *Phys. Rev. D*, 99, 103010
 Norman C. A., Melrose D. B., Achterberg A., 1995, *ApJ*, 454, 60
 Pillepich A., Nelson D., Truong N., Weinberger R., Martin-Navarro I., Springel V., Faber S. M., Hernquist L., 2021, *MNRAS*, 508, 4667
 Plotko P., van Vliet A., Rodrigues X., Winter W., 2022, arXiv e-prints, p. arXiv:2208.12274
 Predehl P., et al., 2020, *Nature*, 588, 227
 Prosin V., et al., 2022, arXiv e-prints, p. arXiv:2208.01689
 Ptuskin V. S., Khazan Y. M., 1981, *Soviet Ast.*, 25, 547
 Ptuskin V., Rogovaya S., Zirakashvili V., 2013, *Adv. Space Res.*, 51, 315
 Recchia S., Gabici S., Aharonian F. A., Niro V., 2021, *ApJ*, 914, 135
 Rieger F. M., Duffy P., 2019, *ApJ*, 886, L26
 Seo J., Kang H., Ryu D., 2021, *ApJ*, 920, 144
 Su M., Slatyer T. R., Finkbeiner D. P., 2010, *ApJ*, 724, 1044
 Völk H. J., Zirakashvili V. N., 2004, *A&A*, 417, 807
 Wang X.-Y., Razzaque S., Mészáros P., Dai Z.-G., 2007, *Phys. Rev. D*, 76, 083009
 Wang J.-S., Reville B., Liu R.-Y., Rieger F. M., Aharonian F. A., 2021, *MNRAS*, 505, 1334
 Wei S.-W., Liu Y.-X., Guo H., Fu C.-E., 2010, *Phys. Rev. D*, 82, 103005
 Zirakashvili V. N., Ptuskin V. S., 2008, *ApJ*, 678, 939
 Zirakashvili V., Ptuskin V., 2018, *Astropart. Phys.*, 98, 21

APPENDIX. MAXIMUM ENERGY LIMIT FROM THE STREAMING INSTABILITY

The maximum rate Γ of the nonresonant streaming instability is given by (Bell 2004)

$$\Gamma = \frac{\sqrt{\pi}J}{c\sqrt{\rho}} = \frac{\eta_{\text{esc}}u^3 e\sqrt{\pi\rho}}{2c\epsilon_{\text{max}}} \quad (1)$$

where ρ is the plasma density, u is the shock speed, and the electric current of energetic particles J was expressed in terms of the parameter η_{esc} that is the ratio of the energy flux of runaway particles with energy ϵ_{max} to the flux of the shock kinetic energy $\frac{1}{2}\rho u^3$.

For the instability to have enough time to amplify the magnetic field from the seed value of B_b to the value of B the rate $\Gamma = \frac{u}{R} \ln \frac{B}{B_b}$ where R is the shock radius. This gives the estimate for the maximum energy (c.f. Zirakashvili & Ptuskin (2008); Bell et al. (2013))

$$\epsilon_{\text{max}} = \frac{e\eta_{\text{esc}}\sqrt{\pi\rho}Ru^2}{2c \ln B/B_b} = \frac{\eta_{\text{esc}}}{2 \ln(B/B_b)} e\sqrt{uL_j c^{-2}} \quad (2)$$

where the shock parameters are expressed in terms of the power of two opposite jets $L_j = \pi\rho u^3 R^2$. Introducing $\beta = u/c$ we obtain the equation (5) in the main text.

This paper has been typeset from a $\text{\TeX}/\text{\LaTeX}$ file prepared by the author.